Journal of Environmental Chemical Engineering 13 (2025) 120217

Contents lists available at ScienceDirect

Journal of Environmental Chemical Engineering

journal homepage: www.elsevier.com/locate/jece

Laboratory evaluation of calcium polysulfide for immobilization of metals from contaminated groundwater under site-specific conditions

Jin Chul Joo [a], Hyeon Woo Go [b], Charles D. Shackelford [c], Kyoungphile Nam [d,*], Hee Sun Moon [e], Dong Jun Kim [f], So-Jeong Kim [g]

[a] Department of Civil and Environmental Engineering, Hanbat National University, Daejeon, 34158, Republic of Korea
[b] Beautiful Environmental Construction, CO., Ltd, Gyeonggi-Do 13207, Republic of Korea
[c] Department of Civil and Environmental Engineering, Colorado State University, Fort Collins, CO 80523-1372, USA
[d] Department of Civil and Environmental Engineering, Seoul National University, Seoul 08826, Republic of Korea
[e] Groundwater Environment Research Center, Geo-Environment Research Division, Korea Institute of Geoscience and Mineral Resources, Daejeon 34132, Republic of Korea
[f] Center of Water Environment & Carbon Assessment, Korea Conformity Laboratories, Incheon 21591, Republic of Korea
[g] Environmental Geology Research Center, Geo-Environment Research Division, Korea Institute of Geoscience and Mineral Resources, Daejeon 34132, Republic of Korea

ARTICLE INFO

Keywords:
Calcium polysulfide (CPS)
Contaminated groundwater
Heavy metals
Metal-sulfide precipitation
Site-specific field soil

ABSTRACT

This study investigated the performance of calcium polysulfide (CPS) for immobilizing mixed heavy metals in acidic–oxidizing groundwater collected from a smelting-impacted refinery in South Korea. A laboratory column experiment was conducted using site-specific soil and groundwater to evaluate CPS transport, redox evolution, metal precipitation, and hydraulic response under realistic geochemical conditions. The injection of CPS rapidly established reducing and alkaline environments, promoting the precipitation of metal sulfides ($MeS_{(s)}$), gypsum, and secondary iron (hydr)oxides while inducing only moderate reductions in hydraulic conductivity. Mass-balance analyses demonstrated nearly complete cadmium sequestration and partial removal of zinc and magnesium, governed primarily by sulfide affinity and solubility equilibria. Mineralogical and spectroscopic characterization confirmed the formation of $ZnS_{(s)}$, $CdS_{(s)}$, and $CaSO_4{\cdot}2H_2O_{(s)}$, whereas microbial community profiling revealed enrichment of sulfur- and iron-metabolizing taxa within CPS-reactive zones, suggesting potential microbial contributions to long-term stability. Compared with previous tests employing clean model sands, the overall removal efficiency in site soil was lower, reflecting the effects of geochemical complexity, competing ions, and localized precipitation. These findings demonstrate that the efficiency and longevity of CPS treatment are controlled by the interplay among metal-specific thermodynamics, site mineralogy, and redox buffering. The results highlight the importance of integrating mass-balance evaluation, mineralogical confirmation, and microbial characterization to accurately assess in-situ performance and to optimize design parameters for sustained sulfide-based remediation of mixed-metal contaminated groundwater.

1. Introduction

In-situ redox manipulation technologies for remediation of heavy metal-contaminated groundwater have been explored extensively, using a range of chemical reductants such as ferrous oxide (FeO), ferrous sulfate ($FeSO_4$), iron sulfide (FeS), sodium dithionite ($Na_2S_2O_4$), and calcium polysulfide (CPS, CaS_x). Among these reductants, CPS has demonstrated excellent effectiveness in reducing and immobilizing hexavalent chromium (Cr^{6+}) by converting Cr^{6+} into the less toxic and sparingly soluble trivalent form, $Cr(OH)_3$, via sulfide-mediated reduction [1–8].

Several field-scale applications in the USA have demonstrated the efficacy of CPS for Cr^{6+} remediation across diverse geochemical settings. Notable examples include the Coast Wood Preserving Superfund Site (Ukiah, CA), where CPS injections have been ongoing since 1999 to achieve regulatory compliance [3], and a former chrome plating facility in Los Angeles, where CPS reduced Cr^{6+} concentrations ranging from 170 to 910 mg/L to below detection limits (< 0.1 mg/L) within a 6.0–7.5 m radius [4]. Other large-scale deployments, such as at the Hanford 100-K Area (Hanford, WA) [2], the Lewis (KS) site [9], and the

* Corresponding author.
E-mail address: kpnam@snu.ac.kr (K. Nam).

https://doi.org/10.1016/j.jece.2025.120217
Received 24 August 2025; Received in revised form 6 November 2025; Accepted 7 November 2025
Available online 8 November 2025

Nevada Environmental Response Trust site [10], further underscore the versatility of CPS for remediation of Cr^{6+} under variable site conditions.

Despite the proven success of CPS in Cr^{6+} remediation, the application and efficacy of CPS for the immobilization of redox-inert, divalent heavy metals (Me^{2+}), particularly in mixed-contaminant systems, remains largely unexplored. Unlike Cr^{6+}, which undergoes redox-driven transformation, Me^{2+} species such as cadmium (Cd^{2+}), copper (Cu^{2+}) and zinc (Zn^{2+}) require sulfide complexation and precipitation as metal sulfides ($MeS_{(s)}$) that are governed by solubility equilibria. Existing research on the potential for CPS to immobilize various Me^{2+} species in mixtures is limited, although preliminary evidence indicates that CPS could facilitate the removal of Me^{2+} through $MeS_{(s)}$ precipitation in subsurface environments [7,11–17]. Upon injection into groundwater, CPS undergoes hydrolysis to release reactive sulfur species (e.g., CaS_2O_3 or H_2S) that react with Me^{2+} to form low-solubility $MeS_{(s)}$, thereby decreasing aqueous concentrations and bioavailability. However, the effectiveness of this mechanism is governed by the solubility product constant (K_{sp}) of $MeS_{(s)}$ and is sensitive to geochemical parameters including pH, oxidation-reduction potential (ORP), and the presence of competing anions (e.g., SO_4^{2-}, Cl^-), especially in mixed-metal plumes typical of smelting sites.

Although increasing evidence suggests that CPS can effectively immobilize Me^{2+}, the broader applicability of CPS to site-specific remediation scenarios is still largely unknown. Soya et al. [11] demonstrated the removal of Cu^{2+}, Ni^{2+}, and Zn^{2+} via pH-controlled sulfidation using calcium sulfide (CaS), a sulfide donor that is chemically similar to CPS, and showed that optimized CaS-to-Me^{2+} molar ratios significantly enhance precipitation efficiency, particularly under acidic conditions that promote CaS hydrolysis and sulfide release. Similarly, Tu et al. [12] assessed the role of CPS in Cd^{2+} stabilization within coastal wetland soils, and identified initial pH increase followed by gradual stabilization as a key factor for determining long-term immobilization. Field observations also support CPS applicability to Cd^{2+}, with one study (New England, USA) showing rapid reductions (< 19 d) in Cd^{2+} concentrations under acidic, oxidizing conditions following CPS injection [18]. However, these studies are limited without field-scale validation for more complex heavy metal mixtures. Moreover, secondary effects such as re-mobilization due to overdosing, rebound in pH, or shifts in ORP have been reported, particularly for Cu^{2+} and Zn^{2+} in systems lacking tight control of redox and sulfur dosing [13,19].

Although recent studies [11–13,19] have advanced understanding of CPS reactivity and metal precipitation in controlled laboratory systems, knowledge of the performance of CPS in remediating mixed-metal plumes with realistic geochemical complexity currently is lacking. Most notably, the interplay between metal-specific K_{sp}, competing contaminants, and subsurface mineralogy can significantly influence Me^{2+} precipitation and long-term stability. Unlike Cr^{6+}, which is governed by redox thermodynamics, Me^{2+} sequestration through sulfide precipitation requires precise control of CPS dosage, contact time, and redox buffering to minimize incomplete precipitation or unintended re-solubilization. Competitive interactions with co-occurring metals and anions, as well as soil mineralogy and pore-scale precipitation, further complicate the performance of CPS in remediating mixed-metal plumes. These factors are particularly relevant in acidic groundwater environments typically associated with smelting facilities, where elevated concentrations of metals and unfavorable redox conditions prevail. Consequently, CPS performance in acidic, site-specific mixed-metal plumes, remains largely unexplored, particularly with respect to metal-selective breakthrough and microbial involvement.

Accordingly, the goal of this study is to evaluate the performance of CPS in immobilizing high-concentration heavy metals in a mixed-contaminant environment, focusing on the use of the site-specific contaminated soil and acidic groundwater (pH = 3.97) from an active smelting facility in South Korea. The specific objectives necessary to achieve this goal are to: (1) investigate the transport behavior of CPS and the subsequent formation of metal sulfide precipitates ($MeS_{(s)}$); (2) assess changes in hydraulic conductivity (K) caused by pore clogging from metal precipitate accumulation; (3) quantify the reactive retention time (longevity) of CPS and the removal efficiencies for multiple heavy metals through mass balance analysis; (4) compare CPS-mediated heavy metal removal in site-specific contaminated soil versus model porous media; (5) examine the influence of metal sulfide solubility (i.e., K_{sp}) on removal efficiency and longevity of CPS; and (6) investigate the microbial community shifts in response to CPS injection.

2. Materials and methods

2.1. Site-specific soil and groundwater

The site-specific soil and groundwater were collected from an active smelting facility in South Korea impacted by heavy metal-laden sludge and leachate. Soil samples were air-dried, sieved through a No. 4 (4.75 mm) mesh, homogenized, and stored at 20°C prior to testing. The detailed mineral composition of the site-specific soil, determined by X-ray fluorescence (XRF) spectroscopy (XRF-1800, Shimadzu, Japan), is presented in Table S1. The results indicate that the soil is dominated by SO_3 (75.5 mass%), ZnO (13.2 mass%), and CaO (6.51 mass%), with minor fractions of Na_2O (2.75 mass%), MnO (0.46 mass%), and SiO_2 (0.25 mass%). This characterization confirms that the site-specific soil is rich in sulfate and zinc, reflecting prolonged accumulation of smelting residues and exposure to acidic leachate. The particle-size distribution (Fig. S1) indicates that ~ 85 % of the equivalent particle diameters are within the 0.25–2.0 mm range, which results in the soil being classified as poorly graded sand (SP) according to the Unified Soil Classification System [20]. Physical properties of the soil are summarized in Table S2.

Heavy metal concentrations in the soil were determined using the Environmental Standard Test Method in Korea [21]. Following freeze-drying, soil samples were finely ground, and 0.1 g was digested at 150°C for 1.0 h with a 5-mL solution comprising nitric acid (HNO_3), hydrochloric acid (HCl), and hydrofluoric acid (HF) in a 3:2:1 HNO_3:HCl:HF ratio by volume using a microwave digestion system (Titam MPS, PerkinElmer, USA). After cooling, 10 mL of 4 % boric acid (H_3BO_3) solution was added, and the mixture underwent further microwave treatment at 160°C for 0.5 h. The digested sample then was diluted with 1 % HNO_3 to a final volume of 20 mL, which served as a stock solution. Inductively Coupled Plasma-Optical Emission Spectroscopy (ICP-OES) (iCAP PRO, ThermoFisher Scientific, USA) was used to measure the concentrations of several metals, including Al, As, Ca, Cd, Cu, K, Mg, Mn, Na, Pb, and Zn. The resulting values for these metals in terms of soil concentrations except for Al, Ca, K, Mg, and Na, which were either not present or were present at negligible levels, are shown in Table S3. In particular, the concentration for Zn of 8792 mg/kg significantly exceeds the maximum regulated concentration of 5000 mg/kg based on the Korean Standards for Soil Contamination Countermeasures [22], thereby confirming soil contamination by heavy metal sludge and leachate resulting from the smelting refining processes. This high concentration of Zn represents an environmental impact concern due to metal mobility.

Groundwater samples collected from the study site exhibited strongly acidic (pH = 3.97) and oxidizing (ORP = 180 mV) conditions, with elevated concentrations of multiple heavy metals, predominated by Zn (5560 mg/L) and Cd (143 mg/L) (Table S4). The influent used in the column tests was likewise acidic, oxidizing, and rich in sulfate (SO_4^{2-} = 11,800 mg/L), with an electrical conductivity (EC) of 1085 μS/mm and dissolved oxygen (DO) of 4.11 mg/L. Major anions and cations included Cl^- (64.1 mg/L), NO_3^- (19.2 mg/L), HCO_3^- (12.8 mg/L), Na^+ (221 mg/L), K^+ (75.2 mg/L), Ca^{2+} (454 mg/L), and Mg^{2+} (516 mg/L), and sulfide was below detection. Dissolved inorganic carbon (DIC) and dissolved organic carbon (DOC) were not analyzed, since the levels of DIC and DOC were expected to be negligible in this oxidizing, low-alkalinity groundwater.

Although the overall chemical composition of the site-specific groundwater is broadly comparable to that of the simulated groundwater used by Joo et al. [17], with an initial pH of 4.7 and concentrations for Zn and SO_4^{2-} of 10000 mg/L and 15000 mg/L, respectively, the concentrations for Zn of 5560 mg/L and SO_4^{2-} of 11800 mg/L based on the field-collected groundwater samples are lower by factors of 1.8 and 1.3, respectively. In addition to Zn, the field groundwater comprised appreciable concentrations of other heavy metals, including Cd, Cu, Mn, Mg, and Pb. This multi-metal contamination profile is consistent with previous reported compositions of smelting-impacted groundwaters, which often include elevated concentrations of Cd, Ni, Pb, and Zn [23, 24]. The existence of multiple Me^{2+} in an acidic, oxidizing matrix raises concerns regarding competitive interactions during CPS treatment, since these species may compete for available sulfide, thereby influencing both the kinetics and thermodynamic stability of $MeS_{(s)}$ [5,25]. To evaluate these effects, the concentrations of key metals (i.e., Cd, Fe, Mg, and Zn) were quantified using ICP-OES following 0.45 μm filtration of the groundwater samples.

2.2. Calcium Polysulfide (CPS) solution

As described by Joo et al. [17], commercially available, industrial-grade 29 % (w/v) CPS solution (Changsha Easchem Co., Ltd., China) was used in this study. The CPS solution is a yellow-orange aqueous liquid with a density, ρ_{CPS}, of 1.283 Mg/m^3, pH of 10.94, and ORP of −323.4 mV indicating reducing conditions [16]. The higher-than-water density of the CPS solution enhances CPS retention and persistence within subsurface environments, and the complete solubility of the CPS in groundwater facilitates continuous treatment, enabling sustained reactivity for in-situ treatment.

Calcium polysulfide (CaS_x, x = 2–7) comprises calcium-bound polymeric sulfide chains that progressively degrade into shorter-chain species as pH decreases, releasing a suite of sulfur compounds, including polysulfides (e.g., S_5^{2-}, S_4^{2-}), sulfides (e.g., HS^-, H_2S), and oxidized sulfurs (e.g., $S_2O_3^{2-}$, $S_2O_6^{2-}$) [5]. At pH lower than 8.0, sulfide species (e.g., HS^-, H_2S) dominate sulfide speciation, promoting sulfide complexation and rapid precipitation of Me^{2+} as sparingly soluble $MeS_{(s)}$ [5,6,12,17,25]. This sulfide-mediated sequestration is critical for immobilizing Me^{2+} in contaminated groundwater systems. Furthermore, CPS degradation products do not bioaccumulate, thereby offering minimal ecological risk and supporting the environmental compatibility of CPS for field-scale application [7,26].

2.3. Column tests

Following the methodology outlined in Joo et al. [17], a cylindrical acrylic column (80 mm in inner diameter and 500 mm in height (length)) was used in this study. The CPS injection well was centrally positioned at the 250 mm midpoint of the column to facilitate direct injection and uniform dispersion within the upward flowing groundwater. The column was packed with site-specific soil, and three-way valves at several locations along the length of the column enabled sample collection and piezometric head monitoring. A single representative column was operated due to the limited availability of site-specific soil and groundwater, with the experimental design focused on achieving a mechanistic evaluation under field-realistic geochemical conditions. The soil was air-dried but not sterilized to preserve native microbial communities, and no abiotic (sterilized) controls were included. Detailed specifications and schematics are provided in Table 1 and Fig. S2.

Prior to CPS injection, a tracer test using 0.01 M potassium bromide (KBr) solution was conducted to determine the longitudinal dispersivity (α_L) and hydrodynamic dispersion coefficient (D_h) within the column, which served as baseline parameters for assessing CPS-induced transport and permeability changes. The resulting hydraulic and transport parameters, including the pore volume, Darcy flux, seepage velocity, hydraulic conductivity, residence time, and model-derived dispersive properties (D_h, α_L, and column Péclet number) are summarized in Table 1 and illustrated in Fig. S3.

Table 1
Detailed specifications and model parameters for the column tests packed with the site-specific soil.

Model Parameters	Column
Total Volume of Column, V_T (mL)	2510
Cross-sectional Area, A (mm^2)	5020
Pore Volume, PV (mL)	846
Bulk (Dry) Density, ρ_b (Mg/m^3)	1.72
Volumetric Flow Rate, Q (mL/d)	1800
Darcy Flux, q (m/d)	0.358
Residence Time, RT (d)	0.470
Hydraulic Conductivity, K (m/d)	2.16
Seepage Velocity, v_s (m/d)	1.06
Hydrodynamic Dispersion Coefficient, D_h (x 10^{-3} m^2/d), from KBr tracer tests (see Fig. S3)	42.6
Longitudinal Dispersivity, α_L (mm)	40.2
Column Peclet Number, P_L (= $v_s \cdot L/D_h$)	12.4

The testing with CPS followed the tracer test. First, approximately 2.0 pore volumes (1692 mL) of site-specific groundwater were permeated through the column to establish steady-state flow conditions and to flush any residual KBr from the pore water within the soil. Influent conditions were maintained at 15.5°C, consistent with the in-situ groundwater temperature, and oxygen intrusion was minimized by N_2-purged headspace prior to testing. Then, a 58 mL pulse of 29 % (w/v) CPS solution was rapidly injected (≤ 1 min) through the designated injection port (see Fig. S2). This injected volume was selected to achieve an overall CPS concentration of approximately 1.9 % (w/v) across the 846 mL pore volume consistent with the optimal range (1.8–2.0 % w/v) established in Joo et al. [17]. The adopted dosage ensures comparable sulfide availability and reaction conditions, allowing a direct performance comparison under site-specific soil and groundwater conditions.

Following the CPS injection, site groundwater was continuously introduced for an additional 4.0 pore volumes of flow (PVF) to facilitate sulfide-metal reactions and precipitate formation. The CPS injection initiated reactions between dissociated sulfide species and Me^{2+} in the contaminated groundwater, leading to the precipitation of sparingly soluble $MeS_{(s)}$. In addition, Ca^{2+} released from CPS upon reaction with native sulfate (SO_4^{2-}) forms secondary mineral phases such as gypsum ($CaSO_4{\cdot}2H_2O_{(s)}$). These precipitates have the potential to clog pores and alter soil hydraulic conductivity (K). To investigate clogging caused by the precipitation of $MeS_{(s)}$ and secondary phases, three-way valves were incorporated into the column setup to enable liquid sampling and piezometric monitoring at each sampling port. Accordingly, the total head (h_T) at each sampling port and changes in total head ($\triangle h_T$) across subsections were monitored throughout the experiment.

To access geochemical evolution and contaminant immobilization, 10-mL samples were collected periodically from the effluent sampling port, the five designated internal sampling ports, and the effluent collection reservoir (see Fig. S2). Each sample was filtered using a 0.45-μm syringe filter and analyzed for pH, ORP, and EC. Heavy metal concentrations were quantified using ICP-OES, whereas anion concentrations were measured via ion chromatography (940 Professional IC, Vario, Metrohm, Switzerland).

To evaluate heavy metal sequestration following CPS injection, cumulative mass removal and mass balance calculations were performed based on the methodology outlined by Joo et al. [17]. For mass balance evaluation, effluent concentrations were determined as volume-averaged values from the collected reservoir over each sampling interval, whereas concentration profiles along the column represent instantaneous measurements at each sampling port. Internal sampling volumes were incorporated into the cumulative mass calculations, resulting in an overall mass recovery (R) of 98 ± 2 % that represents negligible losses (e.g., due to volatilization or unmeasured sorption).

The mass balance for heavy metals was determined by calculating the cumulative mass of heavy metals entering (M_{in}) and exiting (M_{out}) the column, which were determined based on the measured concentrations in the inflow (C_{in}) and outflow (C_{out}), the groundwater flow rate (Q), the total volume of effluent collected (V_{out}), and the concentrations of heavy metals in the samples (C_{sam}) from the sampling ports (V_{sam} = 10 mL). These parameters were used to quantify the reduction in mass of each heavy metal resulting from CPS injection and retention within the column.

The mass balance for heavy metal removal was calculated using the following equations:

$$\sum_{t=0}^{t} m_{in}(t) = C_{in} \cdot Q_{in} \cdot t \quad (1)$$

$$\sum_{t=0}^{t} m_{out}(t) = C_{out}(t) \cdot V_{out}(t) \quad (2)$$

$$\sum_{t=0}^{t} m_{samples}(t) = \sum_{t=0}^{t} \sum_{i=1}^{i=N} C_{samp,i}(t) \cdot V_{samp,i}(t) \quad (3)$$

$$\sum_{t=0}^{t} m_{removed}(t) = \sum_{t=0}^{t} m_{in}(t) - \sum_{t=0}^{t} m_{out}(t) - \sum_{t=0}^{t} m_{samples}(t) \quad (4)$$

$$R\left(\%\right) = \left(\frac{m_{out} + m_{samples} + m_{removed}}{m_{in}}\right) \times 100 \quad (5)$$

where m_{in}, m_{out}, $m_{samples}$, and $m_{removed}$ are the masses (g) of a heavy metal in the inflow, outflow, sampled aliquots, and sequestered from the aqueous phase, respectively, C_{in} is the constant input concentration of each heavy metal (mg/L), Q_{in} is the constant volumetric groundwater flow rate (mL/d), C_{out} (t) is the volume-averaged output concentration of each heavy metal (mg/L), V_{out} (t) is the cumulative volume of groundwater outflow (mL), N = the number of sampling locations, $C_{samp,\ i}$ (t) and $V_{samp,\ i}$ (t) are the concentration of each heavy metal (mg/L) and the sample volume (= 10 mL) at each sampling site (i) at specified time intervals, respectively, and t is the elapsed time (d).

3. Results and discussion

3.1. Effect of Localized CPS retention on hydraulic conductivity

The spatial and temporal distributions of calcium polysulfide (CPS) transport and associated precipitate formation within the column are illustrated in Fig. 1. Immediately after CPS injection (≤ 0.2 PVF), the denser CPS solution descended to the column bottom under the influence of gravity, initiating localized reactions with groundwater constituents at the base of the column. This behavior is reflected in Fig. 2**a, b**, where a pronounced increase in head loss, -△h_{12} (> 0), and reduction in sectional hydraulic conductivity (K_{12}) were observed within the 0–0.1 m section.

As groundwater injection continued, the initially settled CPS was gradually displaced upward and converged with residual CPS near the injection zone (K_{34}), where further reactions with dissolved species promoted the formation of sparingly soluble $MeS_{(s)}$ (e.g., $CdS_{(s)}$, $ZnS_{(s)}$) and secondary mineral salts such as gypsum ($CaSO_4 \bullet 2H_2O_{(s)}$). Consistent with these processes, K_{34} also declined, and -△h_{34} (> 0) increased, indicating a second precipitate-enriched clogging. Also, a brief increase in K was observed for K_{12} and K_{23} between approximately 1.5 and 2.0 PVF (Fig. 2**a**). This transient rise likely reflects short-term dissolution of soluble phases and reorganization of flow paths during early CPS migration, which temporarily enhanced permeability before subsequent precipitation-induced clogging reduced K.

To relate local changes to bulk seepage behavior, fractional head losses (-△h_i/-△h_T) were calculated and revealed that the -△h_{12} and -△h_{34} sections, comprising less than 40 % of the total column length, accounted for over 60 % of total head loss (Fig. 2**c**). These results confirm that hydraulic resistance was spatially concentrated, forming localized flow constrictions rather than uniform clogging across the column.

Despite these localized permeability reductions and visual evidence of precipitate accumulation (see Fig. 1), overall groundwater flow was not significantly impeded (see Fig. 2**a**). The total harmonic-mean hydraulic conductivity (K_T) decreased from an initial value of 2.15 m/

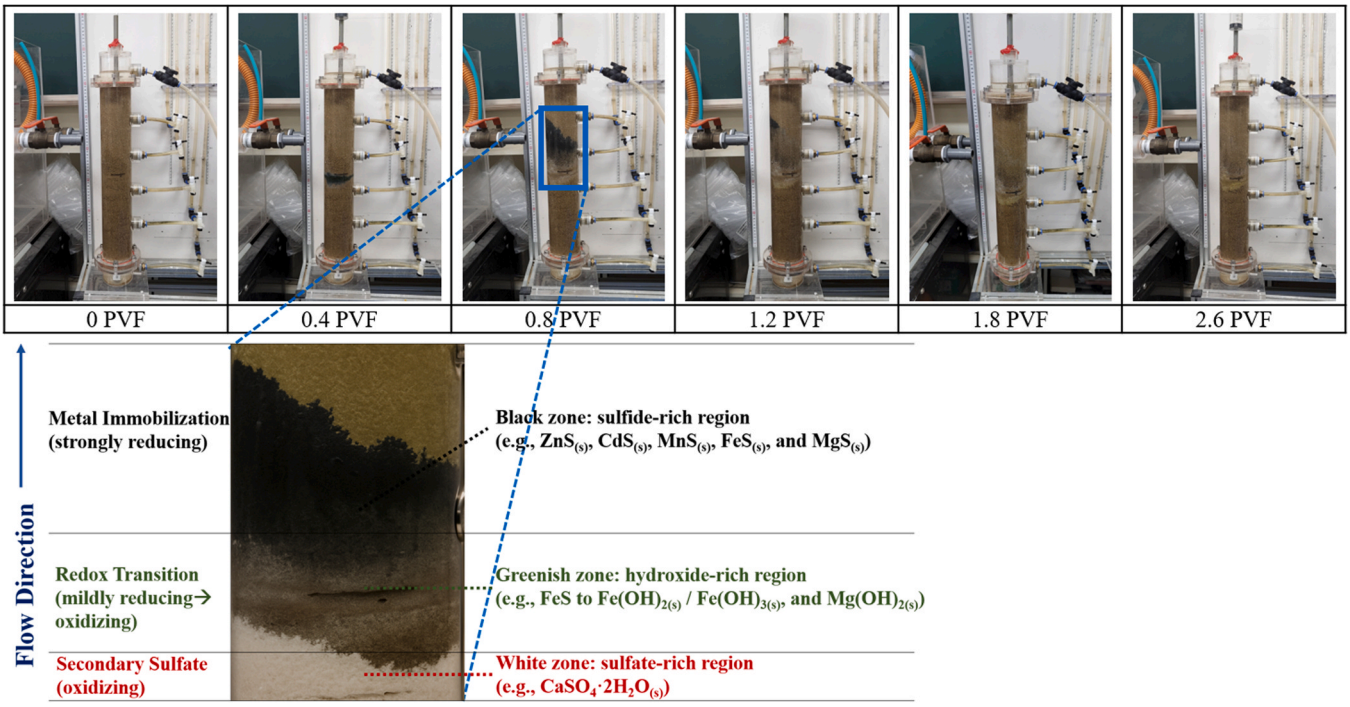

Fig. 1. Pictorial views of calcium polysulfide (CPS) transport and precipitation over time in column packed with site-specific soil. [Note: Color zonation of CPS-treated soil column showing distinct geochemical regions: black (sulfide-rich, $FeS_{(s)}$, $CdS_{(s)}$, $ZnS_{(s)}$), greenish (hydroxide-rich, $Fe(OH)_{3(s)}$, $Mg(OH)_{2(s)}$), and white (sulfate-rich, $CaSO_4 \cdot 2\ H_2O_{(s)}$). The transition between black and white zones indicates overlapping redox gradients and sequential oxidation reactions].

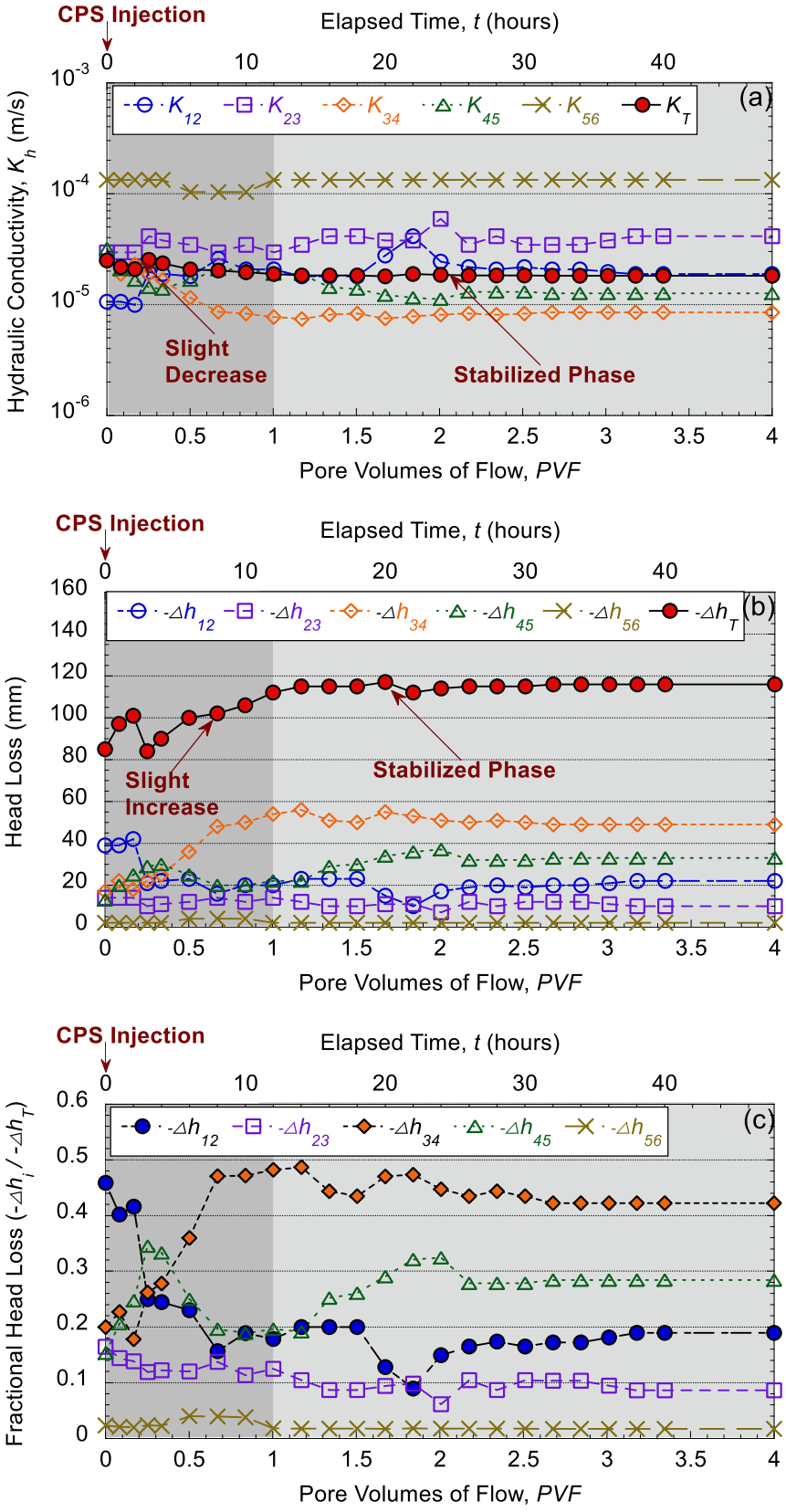

Fig. 2. Changes in the (a) hydraulic conductivity (K), (b) head loss ($-\Delta h$), and (c) fractional head loss in column packed with site-specific soil after calcium polysulfide (CPS) injection. [Note: K_{12}, K_{23}, K_{34}, K_{45}, and K_{56} = hydraulic conductivity values in sections of 1–2, 2–3, 3–4, 4–5, and 5–6, respectively, and K_T = total hydraulic conductivity for the entire column] [Note: $-\triangle h_{12}$, $-\triangle h_{23}$, $-\triangle h_{34}$, $-\triangle h_{45}$ and $-\triangle h_{56}$ = head difference values in sections of 1–2, 2–3, 3–4, 4–5, and 5–6, respectively, and $-\triangle h_T$ = total head difference for the entire column].

d (2.50 $\times 10^{-5}$ m/s) to 1.57 m/d (1.82 $\times 10^{-5}$ m/s) at 4.0 PVF after CPS injection, reflecting a moderate reduction by a factor of 1.37. This limited decrease in K_T values indicates that the precipitation-induced pore clogging was spatially confined and hydraulically limited, insufficient to impede seepage under the experimental conditions, as reflected in Fig. 2**a**. These findings are consistent with those from previous studies reporting that *in situ* CPS injection, when properly dosed and hydraulically balanced, does not significantly degrade hydraulic performance in porous media [1,17].

3.2. Influence of soil properties on CPS migration

The transport behavior of CPS shown in Fig. 1 is notably different than that observed by Joo et al. [17] based on column tests using a model sand, where the CPS solution initially settled to the bottom of the column, forming a temporary green zone before dispersion and subsequent precipitation of $ZnS_{(s)}$ and gypsum. In contrast, the use of the site-specific soil in this study induced greater lateral retention near the injection zone, limiting vertical migration and resulting in localized zones of persistent reactivity. This behavior can be attributed to early-stage precipitation near the injection zone, which reduced local permeability, combined with the greater textural complexity of the site-specific soil.

Although both the model sand and the site-specific soil are classified as poorly graded sands (SP), the site-specific soil is more well-graded than the model sand used by Joo et al. [17]. The broader particle-size distribution of the site-specific soil relative to that for the model sand used in Joo et al. [17] (see Fig. S1) likely resulted in greater tortuosity, thereby enhancing lateral spreading of CPS. The greater tortuosity and heterogeneity of the site-specific soil relative to the porous media used by Joo et al. [17] are supported by the significantly higher longitudinal dispersivity, α_L, of 40.2 mm observed in this study compared to values of 5.51 mm and 7.94 mm reported by Joo et al. [17] for the model sand and model sand interspersed with clay lenses, respectively, indicating enhanced dispersion and pore-scale variation in this study. Additionally, the differences in particle-size distributions resulted in a significantly lower K_T value for the site-specific soil of 2.16 m/d relative to the K_T values of 69.2 and 26.9 m/d reported by Joo et al. [17] for the model sand and model sand interspersed with clay lenses, respectively. These differences in dispersity and hydraulic conductivity underscore the influence of textural complexity on CPS migration.

The observed differences in CPS migration behaviors between the two studies highlight the critical role of particle-size distribution (Fig. S1) on CPS transport and reactivity. Although the gravitational migration of CPS required 0.2 PVF in this study, which is nearly double the time of $<$ 0.1 PVF reported by Joo et al. [17]. This relative delay reflects increased tortuosity and reduced pore connectivity for the column with the site-specific soil, which hinder uniform CPS distribution and promote preferential accumulation in zones of reduced permeability. Also, the column Péclet number (P_L = 12.4), calculated from measured flow and dispersion parameters, indicates advection-dominated but moderately dispersive transport, consistent with slower gravitational migration and localized accumulation of CPS in low-permeability zones. Thus, the observed retardation reflects both tortuosity-induced path elongation and precipitation-driven pore constriction, which together hinder uniform downward migration and promote preferential CPS retention.

The localized CPS retention facilitated the formation of a broad range of solid phases, including various metal sulfides (e.g., $ZnS_{(s)}$, $CdS_{(s)}$, $MnS_{(s)}$, $FeS_{(s)}$, and $MgS_{(s)}$), sulfates (e.g., $CaSO_4{\cdot}2H_2O_{(s)}$), and hydroxides (e.g., $Fe(OH)_{3(s)}$ and $Mg(OH)_{2(s)}$), as visually manifested by the distinct black, greenish, and white zones (Fig. 1). These zones developed progressively along the flow path, reflecting a reduction–oxidation gradient induced by CPS transport and reaction. The black zone, located near the injection interface, corresponds to strongly reducing, sulfide-rich regions where extensive precipitation of $MeS_{(s)}$ phases ($ZnS_{(s)}$, $CdS_{(s)}$, $FeS_{(s)}$) occurred, promoting early immobilization of redox-sensitive metals. Down-gradient, a greenish transition zone formed under mildly reducing to oxidizing conditions, consistent with the partial oxidation of FeS to $Fe(OH)_2$/$Fe(OH)_3$ and co-precipitation of $Mg(OH)_2$. The white zone, observed further downstream, represents oxidizing, sulfate-rich regions (e.g., $CaSO_4{\cdot}2H_2O_{(s)}$) formed through the reoxidation of reduced sulfur species and coupling with dissolved Ca^{2+}. The fading boundaries between these zones indicate overlapping redox fronts and concurrent reactions involving Fe^{2+}/Fe^{3+} cycling and sulfide reoxidation. Although these interpretations are based primarily on visual and geochemical evidence, subsequent mineralogical analyses (XRD, SEM–EDS) were conducted to confirm the presence and distribution of specific mineral phases. Collectively, the observed zones reflect sustained interactions between residual CPS and dissolved constituents under field-representative geochemical conditions.

With continuous groundwater inflow, CPS was gradually displaced upward but remained largely confined to the injection zone, with no breakthrough detected at the column outlet. As illustrated in Figs. 1 and 2, CPS preferentially accumulated in mid-column zones with reduced hydraulic conductivity (e.g., K_{34}), where precipitation further limited mobility. These findings suggest that precipitation-induced reductions in permeability, albeit relatively minor in magnitude, strongly influenced CPS migration, and emphasize the importance of considering site-specific soil structure and geochemical conditions when designing effective CPS-based remediation strategies.

3.3. Chemical properties of precipitates

The physicochemical properties of the mineral phases formed during CPS treatment were characterized using scanning electron microscopy coupled with energy-dispersive X-ray spectroscopy (SEM-EDS), X-ray diffraction (XRD), and X-ray photoelectron spectroscopy (XPS) (Fig. 3). The analyzed sample was obtained from the lower section ($\leq$ 0.20 m) of the column, corresponding to the initial CPS settling zone and early-stage reaction front. Although more pronounced visual accumulation occurred in the mid-column region (Fig. 1), the lower zone contained dispersed precipitates representative of early reactions between CPS and groundwater constituents. Similar early-stage precipitation near the column base also has been reported in previous CPS studies (e.g., [17, 27]), supporting the selection of this zone for detailed mineralogical characterization.

SEM imaging revealed heterogeneous mineral deposits distributed across soil grain surfaces, while EDS spectra confirmed the presence of CPS-relevant elements including Ca, Cd, Mg, Mn, S, Si, Fe and Zn. Elemental mapping further revealed spatial co-localization of Ca, S, and Zn, indicating potential zones of metal-sulfur interaction and concurrent precipitation of Ca- and Zn-bearing phases.

XRD analysis identified gypsum ($CaSO_4{\cdot}2H_2O_{(s)}$) as the dominant crystalline phase, with additional peaks corresponding to elemental sulfur ($S_{8(s)}$) and zinc sulfide ($ZnS_{(s)}$). The detection of $ZnS_{(s)}$ supports the thermodynamically favored precipitation of Zn^{2+} via sulfide complexation, even in the presence of excess sulfate. Notably, $CdS_{(s)}$ was not detected in the bulk XRD patterns, likely due to the low crystallinity and trace abundance relative to major phases such as gypsum and $ZnS_{(s)}$.

High-resolution XPS analysis provided additional insight into the binding environments of key elements. Sulfur 2p spectra exhibited characteristic signals attributable to $CaSO_{4(s)}$, $S_{8(s)}$, and $ZnS_{(s)}$, whereas Zinc 2p spectra confirmed the predominance of $ZnS_{(s)}$ over $ZnSO_{4(s)}$, especially under moderately acidic conditions (pH $\leq$ 5). Cadmium 3d spectra revealed well-defined peaks attributed to Cd–S bonding, and EDS elemental mapping showed spatial co-localization of Cd and S, supporting the formation of poorly crystalline $CdS_{(s)}$ that remained below the XRD detection limit. Although Cd removal exceeded 99 %, the absence of crystalline CdS peaks in the XRD also may reflect partial Cd immobilization through surface complexation or co-precipitation with $ZnS_{(s)}$ or $FeS_{(s)}$. These complementary mechanisms, together with

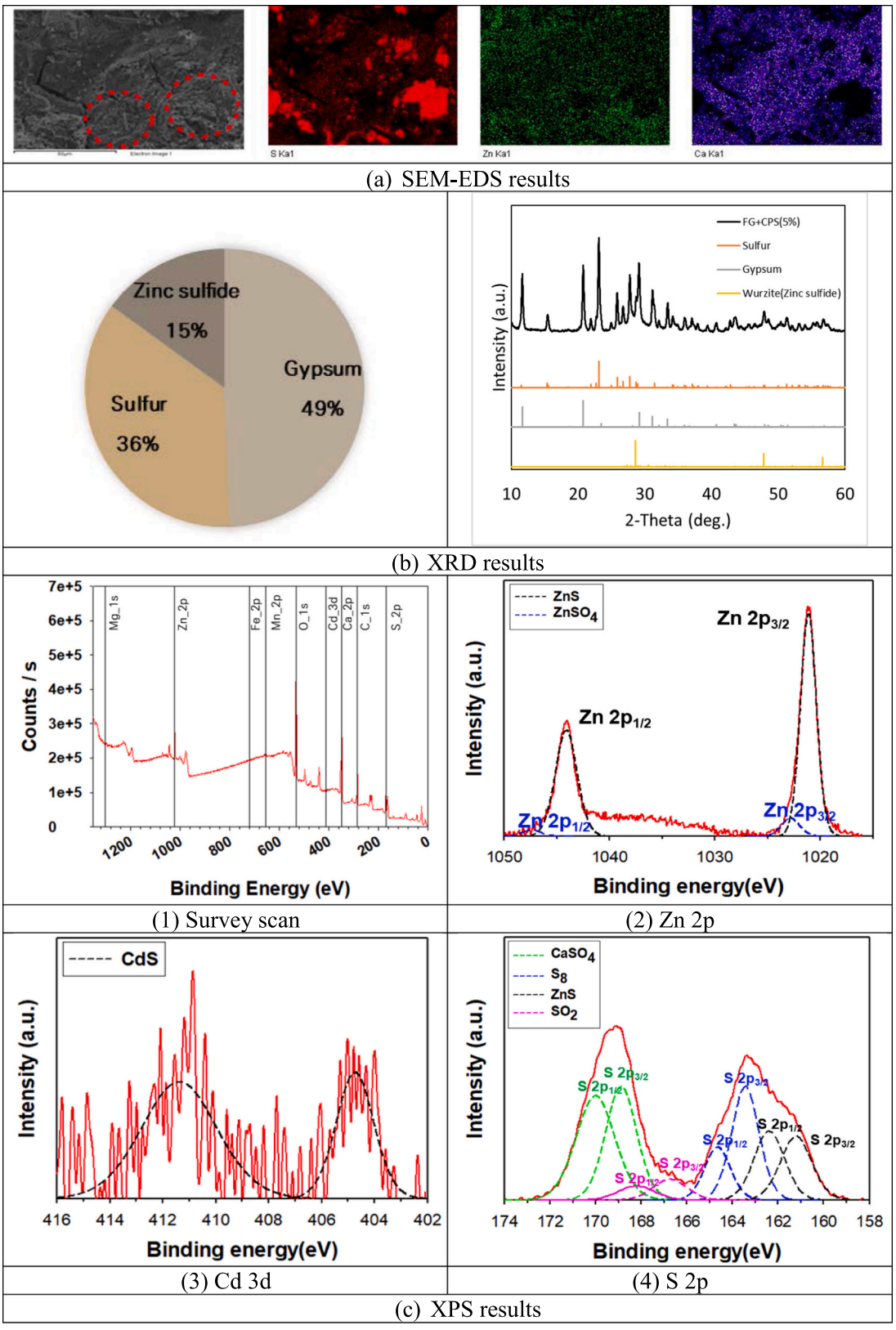

Fig. 3. Results of SEM-EDS, XRD, and XPS analyses for calcium polysulfide (CPS) precipitates collected from soil samples at lower depths (≤ 0.20 m) in the column packed with the site-specific soil. [Note: (a) SEM–EDS mapping confirms co-localization of S, Zn, and Ca in precipitate-enriched zones; (b) XRD pattern showing the coexistence of gypsum ($CaSO_4{\cdot}2\,H_2O_{(s)}$), $ZnS_{(s)}$ (wurtzite), and elemental sulfur (S_8). The absence of $CdS_{(s)}$ reflections is attributed to its low abundance and poor crystallinity, below the XRD detection limit (~1–3 wt%). The phase composition (gypsum 49 %, sulfur 36 %, ZnS 15 %) was estimated semi-quantitatively from relative XRD peak intensities of ZnS(111) ($2\theta \approx 28.5^\circ$) and gypsum(020) ($2\theta \approx 11.6^\circ$); (c) High-resolution XPS spectra for Zn 2p, S 2p, and Cd 3d regions. The S 2p envelope comprises contributions from sulfide (161.8 eV), elemental sulfur (163.7 eV), and sulfate (168.5 eV). The S component likely represents a mixture of residual CPS decomposition products and reoxidized sulfide under localized oxidizing conditions.].

sulfide precipitation, account for the nearly complete sequestration of Cd^{2+} observed in the column.

Collectively, the SEM-EDS, XRD, and XPS data confirm that Cd^{2+} and Zn^{2+} were primarily immobilized through the formation of $CdS_{(s)}$ and $ZnS_{(s)}$, respectively, while Ca^{2+} participated in secondary precipitation as gypsum. The selective formation of $MeS_{(s)}$ reflects the strong affinity of Me^{2+} for reduced sulfide species and the thermodynamic stability of the corresponding $MeS_{(s)}$. These findings reinforce the role of CPS as an effective reductant for *in situ* immobilization of both redox-sensitive and redox-inert metals in contaminated groundwater systems.

3.4. Column effluent concentrations

3.4.1. Cadmium, magnesium, and zinc

Temporal variations in the effluent concentrations for Cd, Mg, and Zn following CPS injection are illustrated in Fig. 4**a,b**. A noticeable decline in heavy metal (Cd, Zn) concentrations beginning at ~ 0.2–0.4 PVF is observed (see Fig. 4**a**), indicating rapid reaction between the injected, reduced sulfide species and dissolved metal cations, although removal efficiencies varied substantially by metal. For instance, Cd concentrations decreased by over 99 % at 1.0 PVF, whereas the maximum reduction for Zn concentrations was less than 72 % at 1.2 PVF. Removal of Mg was less effective, with a decrease of only 42 % at 0.85 PVF (see Fig. 4**b**). Also, the reactive retention time of CPS also varied by metal. For example, Cd concentrations remained continually low throughout the test duration, whereas Mg and Zn concentrations stabilized before rebounding to nearly initial levels at ~ 2.2 and 3.4 PVF, respectively. These differences suggest that the sequestration efficiency of CPS is strongly dependent on metal-specific precipitation kinetics and thermodynamic constraints.

Redox-inert transition (d-block) metal cations, such as Cd^{2+} and Zn^{2+}, readily form sparingly soluble $MeS_{(s)}$ through strong covalent interactions with reduced sulfide species (HS^-/S^{2-}) rather than through direct redox transformations [28]. Consistent with Hard–Soft Acid–Base (HSAB) considerations, these intermediate soft cations (Cd^{2+}, Zn^{2+}) with relatively small ionic radii and moderate electronegativity show strong affinity for soft-base sulfide, promoting the formation of highly insoluble $CdS_{(s)}$ and $ZnS_{(s)}$ [29]. In contrast, the hard-acid Mg^{2+} interacts preferentially with oxygen donors (e.g., OH^-, CO_3^{2-}), rendering $MgS_{(s)}$ thermodynamically unstable in aqueous systems and prone to hydrolysis to $Mg(OH)_{2(s)}$. Accordingly, sulfide precipitation typically is more effective and selective than hydroxide precipitation for removing soft heavy metals such as Cd and Zn from mixed solutions [29,30]. While Mg removal in this study is mainly attributed to hydroxide precipitation, minor contributions from adsorption or co-precipitation with other metal (hydr)oxides cannot be entirely excluded.

These HSAB-governed preferences are reinforced by solubility controls. For example, metals that form very low-solubility sulfides (e.g., 1.0×10^{-28} for $CdS_{(s)}$ and 1.6×10^{-23} for $ZnS_{(s)}$) exhibit strong thermodynamic driving forces for precipitation and, therefore, higher removal efficiencies under the acidic conditions relevant to CPS treatment. By contrast, metals such as Mn^{2+} and Mg^{2+}, which form more soluble sulfides (e.g., 3.2×10^{-14} for $MnS_{(s)}$ and 5.0×10^{-11} for $MgS_{(s)}$) or revert to more soluble hydroxides (e.g., 2.2×10^{-5} $Mn(OH)_{2(s)}$ and 5.0×10^{-12} for $Mg(OH)_{2(s)}$), are less amenable to sulfide-driven removal under comparable geochemical conditions [25].

Consequently, the differences in K_{sp} values among $MeS_{(s)}$ species plays a critical role in governing the precipitation behavior and, by extension, the overall effectiveness of CPS remediation. Metals such as Cd^{2+} and Zn^{2+}, which form $MeS_{(s)}$ with exceptionally low K_{sp} values, reflect strong thermodynamic favorability for sulfide precipitation and, therefore, higher removal efficiencies. In contrast, metals such as Mn^{2+} and Mg^{2+} form $MeS_{(s)}$ with substantially higher K_{sp} values, rendering sulfide precipitation less favorable under comparable geochemical conditions. These differences underscore the critical role of sulfide chemistry and metal-specific solubility in influencing the selectivity and effectiveness of CPS treatments [25,31]. Accordingly, consideration of metal-specific K_{sp} values is essential for predicting CPS performance and for designing CPS-based optimized remediation strategies in environments impacted by mixed-metal contamination.

3.4.2. Iron

Within the CPS retention zone, the introduction of CPS establishes a highly reducing environment, facilitating the reduction of ferric iron (Fe^{3+}), commonly present as iron (hydr)oxides such as ferrihydrite, goethite, or hematite, to ferrous iron (Fe^{2+}) [32]. This reductive dissolution increases the concentration of Fe^{2+} in pore water, which subsequently appears in the effluent, as illustrated in Fig. 4**b**. However, as Fe^{2+} migrates beyond the strongly reducing CPS retention zone into regions with weaker reducing or mildly oxidizing conditions, Fe^{2+} undergoes re-oxidation to Fe^{3+}, leading to the precipitation of newly formed iron (hydr)oxides. This cycle of reduction, elution, oxidation, and reprecipitation explains the transient increase in Fe concentrations, followed by a subsequent decline as Fe becomes immobilized again.

Near the CPS injection zone, strongly reducing zones were identified by low ORP values (≤ -100 mV), elevated Fe^{2+} concentrations, and black coloration indicative of metal sulfide formation, whereas weaker reducing zones exhibited higher ORP (approaching 180 mV) and Fe(III)-(hydr)oxide precipitates (Fig. 1). These patterns underscore the dynamic behavior of iron under sulfur-mediated redox gradients and highlight the dependence of Fe mobility on the spatial extent and persistence of the reducing conditions established by CPS. The response of iron-bearing phases to CPS treatment is influenced by not only mineralogical characteristics and redox potential but also site-specific geochemical complexity, which affects the speciation and reactivity of sulfide species.

3.4.3. Calcium and sulfate

Following CPS injection, Ca^{2+} concentrations in the effluent exhibited a pronounced increase after ~ 0.3 PVF (Fig. 4**c**). This increase is directly attributed to the dissociation of CPS, which released Ca^{2+} and reduced sulfide species into pore water. The elevated Ca^{2+} then reacted with SO_4^{2-} present in the site-specific groundwater, leading to the precipitation of gypsum that depended on local saturation indices and ionic strength conditions. This reaction resulted in a transient concentration trend, whereby Ca^{2+} concentrations initially increased due to CPS dissolution but subsequently decreased via precipitation of gypsum. This contrasting concentration behavior persisted until ~ 3.0 PVF, coinciding with the inferred depletion of reactive CPS. After CPS depletion, the release of Ca^{2+} diminished, and SO_4^{2-} concentrations returned to baseline levels observed in the inflow groundwater. These observations suggest that CPS dissociation persisted until ~ 3.0 PVF, maintaining SO_4^{2-} reactivity over this period.

While the synchronous behavior of Ca^{2+} and SO_4^{2-} offers useful insight into CPS longevity and geochemical reactivity, interpreting CPS persistence based solely on these trends may oversimplify the underlying processes. Additional mechanisms, such as competitive sulfate sorption onto mineral surfaces, complexation with Fe^{2+}/Fe^{3+}, or microbial sulfate reduction, also could influence sulfate kinetics and should be considered when evaluating sulfur speciation and transformation in CPS-treated systems.

3.4.4. pH and ORP

As shown in Fig. 4**d**, the injection of CPS induced a gradual increase in pH and a corresponding decrease in ORP, indicating the establishment of strongly reducing and alkaline conditions within the soil column. This redox shift is attributable to the dissociation of CPS, which releases hydroxide (OH^-) and reduced sulfide species (S^{2-}, HS^-, and H_2S), collectively driving the system toward higher alkalinity and lower redox potential (i.e., $S_x^{2-} + H_2O \rightarrow HS^- + OH^- + S_{x-1}^0$). These reducing conditions facilitated the precipitation of $MeS_{(s)}$, effectively immobilizing dissolved heavy metals. However, beyond ~ 1.7 PVF, a gradual decline in pH is observed, which is attributed to continued metal-sulfide

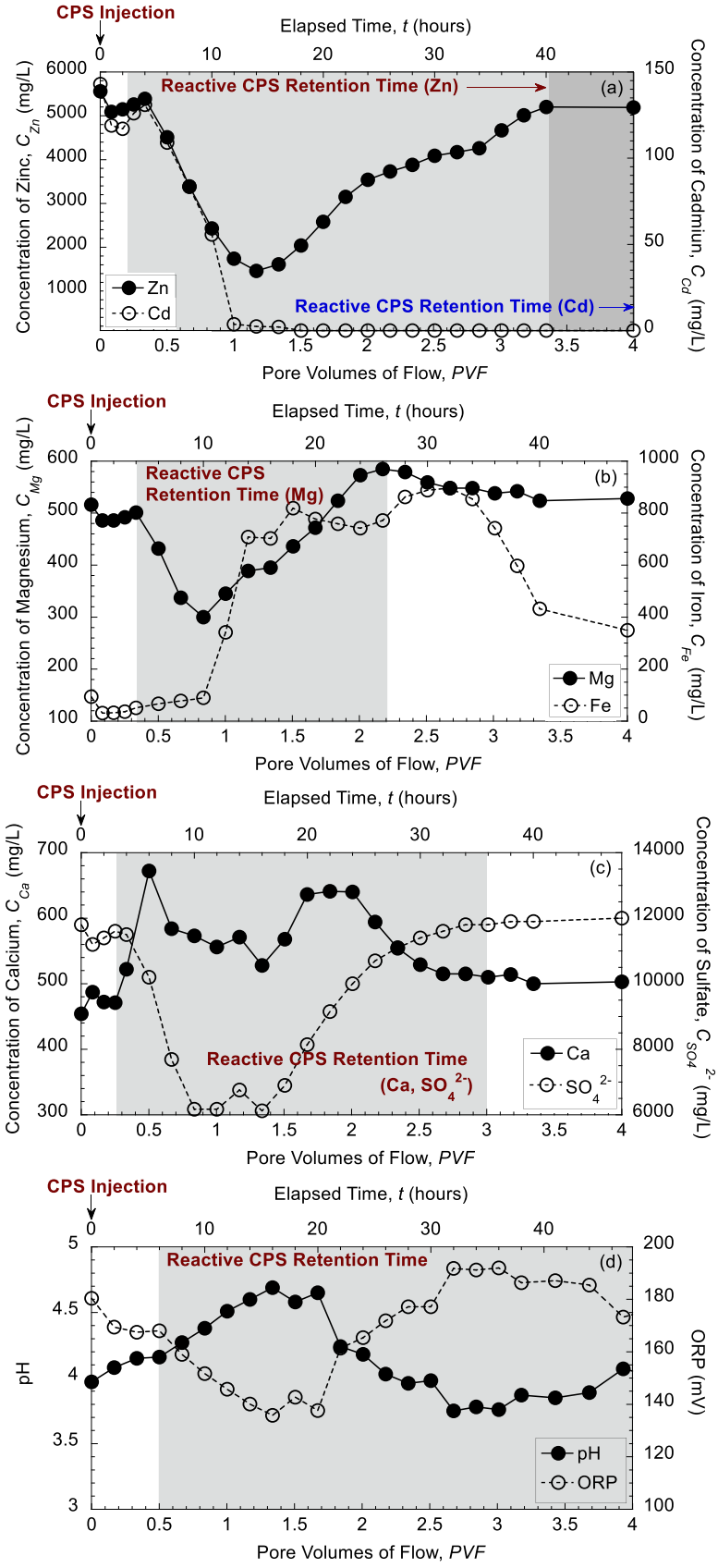

Fig. 4. Temporal variations in effluent concentrations, pH, and ORP from a column packed with site-specific soil and permeated with site-specific groundwater as a function of pore volumes of flow following calcium polysulfide (CPS) injection.

precipitation reactions that release protons (i.e., $Me^{2+} + H_2S \rightarrow MeS_{(s)} + 2H^+$). As H^+ accumulated, the buffering capacity provided by OH^- diminished, leading to pH stabilization at ~ 4.0 PVF. This inflection point is interpreted as the exhaustion of reactive sulfide species and the cessation of dominant sulfide-mediated precipitation processes.

Simultaneously, ORP values continued to decline during early stages of CPS injection as reduced sulfide species reacted with native oxidants, including DO, ferric iron (Fe^{3+}), and manganese oxides. As reflected in Fig. 4**d**, these redox transformations further contributed to the reductive dissolution of iron (hydr)oxides ($Fe^{3+} \rightarrow Fe^{2+}$), which not only increased Fe^{2+} concentrations in the effluent (Fig. 4**b**), but also produced OH^-, buffering the pH against rapid decrease. Both pH and ORP subsequently stabilized at ~ 4.0 PVF, marking the end of the reactive CPS phase and the reestablishment of near-equilibrium geochemical conditions within the column. These coupled trends demonstrate that variations in pH and ORP serve as reliable indicators of redox progression and sulfide reactivity during CPS treatment.

3.5. Mass balance

As shown in Fig. 5, the cumulative mass of Mg and Zn removed stabilized after ~ 2.2 and 3.4 PVF, respectively, whereas Cd removal continued until 4.0 PVF without evidence of stabilization. These patterns are consistent with the effluent concentration trends (Fig. 4**a,b**), wherein Mg and Zn concentrations initially declined but subsequently increased to near-baseline levels at their respective thresholds. In contrast, Cd concentrations decreased by over 99 % at 1.0 PVF and remained low throughout the test duration. The early plateau in Mg and Zn removal suggests that the formation of $MeS_{(s)}$ was limited by both availability and affinity of reactive sulfide species derived from the injected CPS, indicating that these metals reached a stoichiometric or kinetic threshold beyond which further removal was constrained.

As illustrated in Fig. 5**d**, the observed threshold behavior implies that additional CPS dosing would be required to achieve continued Mg and Zn sequestration. In contrast, Cd removal persisted throughout the test due to a lower K_{sp} for $CdS_{(s)}$ and the higher affinity for reduced sulfide species. Although cumulative removal among the three metals was initially similar, divergence occurred beyond ~1.3 PVF, highlighting distinct sulfide affinity and metal-specific sulfide demand. These results underscore the importance of considering individual metal chemistry, particularly K_{sp}, sulfide affinity, and precipitation kinetics, when designing CPS-based remediation strategies for complex multi-contaminant systems.

In field applications, where the transport and reactivity of CPS are influenced by subsurface heterogeneity and geochemical buffering, the observed limitation in Mg and Zn removal suggests that a single injection event may be insufficient to ensure sustained treatment. Thus, optimization of both dosage and injection frequency is critical to extend the reactive lifespan and enhance long-term removal efficiency of CPS, particularly for metals with higher solubility and/or lower sulfide reactivity.

Further comparison of the results of this study versus those reported by Joo et al. [17] reveals significant differences in cumulative mass removal of metals (Fig. 6). Mass removal efficiencies in the current study were notably lower, reflecting the influence of the site-specific soil and groundwater. Specifically, the presence of competing metal cations in both the soil matrix (Table S2) and groundwater (Table S3) reduced the availability of reactive sulfide species for target metals. This competitive environment limited sulfide precipitation of Cd^{2+}, Mg^{2+}, and Zn^{2+}, ultimately diminishing treatment efficiency. Nonetheless, CPS was preferentially consumed by metals exhibiting stronger affinity for sulfide species, primarily those forming precipitates with lower K_{sp}, consistent with observed selectivity in $MeS_{(s)}$ formation.

3.6. Influence of metal sulfide solubility (K_{sp}) on removal efficiency and longevity of CPS

The K_{sp} of $MeS_{(s)}$ plays a critical role in controlling metal immobilization via sulfide precipitation. As shown in Fig. 7, metals forming less soluble sulfides (i.e., lower K_{sp} or higher pK_{sp}, where $pK_{sp} = -\log(K_{sp})$), such as $CdS_{(s)}$ and $ZnS_{(s)}$, achieved greater maximum mass removal efficiencies and more prolonged CPS longevity compared to those for $MgS_{(s)}$, which is thermodynamically less stable and more prone to dissolution. These trends reflect the greater persistence and lower solubility of $CdS_{(s)}$ and $ZnS_{(s)}$ under conditions of limited sulfide availability.

The effectiveness of CPS thus depends on the capacity of dissociated sulfide ions (S^{2-}, HS^-, and H_2S) to reach concentrations sufficient to exceed the solubility thresholds for the target $MeS_{(s)}$. In systems where pK_{sp} values are high, metal ions are more readily precipitated at lower sulfide concentrations, resulting in more efficient immobilization and longer reactive persistence. Conversely, metals with low pK_{sp} values require higher sulfide activity for precipitation and are more susceptible to incomplete removal under competitive geochemical influences.

Although K_{sp} provides a useful baseline for estimating sulfide precipitation, actual CPS treatment outcomes are governed by dynamic groundwater conditions, such as pH variations, redox potential (Eh), and the presence of competing cations or complexing ligands, all of which can significantly influence precipitation kinetics, metal speciation, and bioavailability. Thus, sole reliance on K_{sp} may oversimplify field performance. These thermodynamic trends are consistent with stability relationships via Pourbaix diagrams, wherein pH and Eh control sulfide speciation and precipitation favorability. As emphasized by Zhang et al. [19], selective precipitation of metals via sulfide pathways is governed by not only intrinsic K_{sp} but also operational parameters such as CPS dosing rate, pH, Eh, and sulfide oversaturation.

In addition, excessive CPS dosing beyond stoichiometric requirements can induce unintended side effects, including secondary mineral formation, and redox disruption. Therefore, optimization of CPS application must strike a balance between exceeding solubility thresholds and avoiding adverse secondary reactions. Although this study does not fully quantify all site-specific variables, the observed relationship between pK_{sp}, removal efficiency, and CPS longevity illustrated in Fig. 7 provides a useful framework for designing more effective, metal-specific remediation strategies.

In the present mixed-metal system, pK_{sp} provides a practical metric for interpreting competition, i.e., metals forming less soluble sulfides preferentially consume the majority of available reduced sulfur until sulfide activity declines below the precipitation thresholds. Although K_{sp} alone does not capture kinetic or redox buffering effects, coupling with observed breakthrough ordering, rebound PVF, and plateaus of cumulative mass removal yields a coherent, semiquantitative analysis of competition. Future work will employ composition-controlled groundwaters and soils to derive metal-specific competition factors (e.g., pK_{sp}-weighted sulfide demand curves) for Cd-Zn-Mg mixtures under site-relevant pH-ORP conditions.

3.7. Microbial community of CPS-treated soil column

Microbial contributions to heavy metal stabilization during CPS treatment were evaluated via 16S rRNA gene-based community profiling across five depth intervals (C1–C5) of the CPS-treated soil column. Between 27,546 and 40,711 high-quality sequences were obtained per depth layer (C1–C5), enabling robust characterization of microbial assemblages. Alpha diversity indices (Table S5) revealed a pronounced decline in species richness (Chao1, ACE) and diversity (Shannon, Simpson) within the 200–500 mm depth range, corresponding to the zones of active CPS reactivity and precipitation. These trends suggest that sulfur-induced geochemical perturbations exerted strong selective pressures, favoring specialized taxa adapted to redox-dynamic

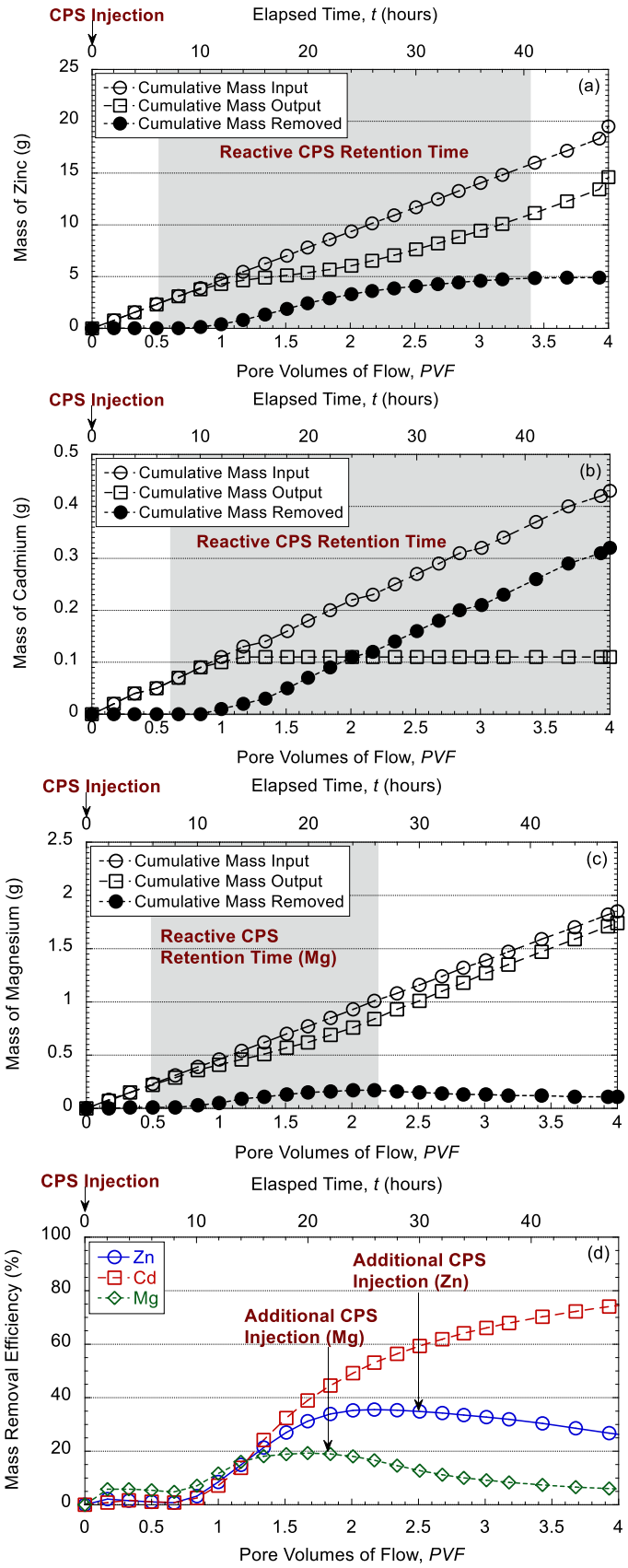

Fig. 5. Cumulative mass breakthrough and corresponding removal efficiencies of major heavy metals as a function of pore volumes of flow following calcium polysulfide (CPS) injection: (a) Zn, (b) Cd, (c) Mg, and (d) mass removal efficiency (%).

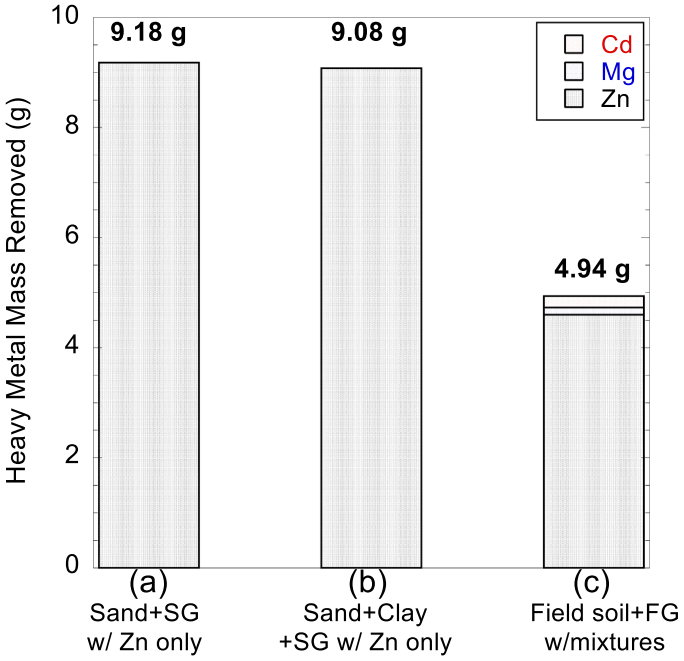

Fig. 6. Comparison of heavy metal removal after three pore volumes of flow following calcium polysulfide (CPS) injection at 1.8 % concentration: (a) and (b) results from Joo et al. [17] using simulated groundwater (SG) with columns packed with model sand only and model sand with interspersed clay lenses, respectively; (c) results from this study using site-specific soil and field groundwater (FG).

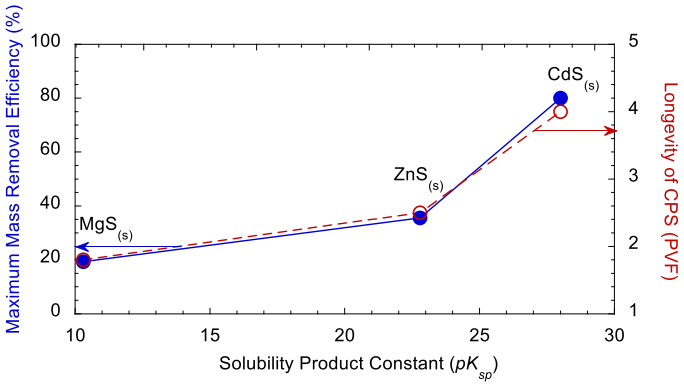

Fig. 7. Comparison of maximum mass removal efficiency (%) and longevity of calcium polysulfide (CPS) in pore volumes of flow (PVF) after CPS injection in column packed with field soil at steady state [Note: K_{sp} values for $ZnS_{(s)}$, $CdS_{(s)}$, and $MgS_{(s)}$ are 1.6×10^{-23}, 1.0×10^{-28}, and 5.0×10^{-11}, respectively.].

environments and reducing microbial evenness in high-activity zones.

Community composition analysis using Bray-Curtis dissimilarity clustering (Fig. S4) revealed distinct microbial assemblages between the mid-column CPS-reactive zones (C3 and C4) and the surrounding layers (C1, C2, and C5). Notably, the CPS-active zones were enriched in members of the genus *Alicyclobacillus*, which is known for oxidizing reduced sulfur and iron compounds under acidic or microaerophilic conditions [33]. Additionally, *Desulfitobacterium*, a strict anaerobe capable of utilizing metals and sulfur compounds as terminal electron acceptors, comprised 11.7 % of the microbial community in C4. The co-occurrence of these taxa suggests that localized reducing conditions promoted the proliferation of sulfur-oxidizing and metal-reducing bacteria potentially involved in $MeS_{(s)}$ formation and redox buffering.

In contrast, the layers of C1 and C2 were dominated by *Thiomonas delicata* (99 % sequence identity), a moderate acidophile commonly associated with arsenic- and sulfur-rich acidic mine drainage environments [34]. The marked decline in *Thiomonas* abundance in the CPS-reactive zones (C3 and C4) is likely attributable to a shift from oxidizing to reducing conditions and the depletion of oxidized sulfur substrates following CPS injection. The co-enrichment of sulfur-oxidizing and sulfate- or metal-reducing microorganisms in CPS-impacted zones suggests a synergistic interplay between biotic and abiotic sulfur cycling. *Alicyclobacillus* may contribute to sulfur reoxidation (e.g., $S^0_{x\text{-}1}$ to SO_4^{2-}), while *Desulfitobacterium* may promote reductive metal immobilization by generating sulfide.

Although functional gene (e.g., *dsrA*, *soxB*) or metabolite-level confirmation (e.g., H_2S, Fe^{2+}) was beyond the scope of this study, the convergence of taxonomic and geochemical evidence supports a hypothesis of microbially assisted stabilization within CPS-treated zones. Such redox-coupled microbial consortia may enhance the longevity of metal sulfide precipitates by sustaining localized reducing microenvironments and replenishing sulfide through continued dissimilatory sulfate reduction. Conversely, if environmental conditions shift toward oxidation (e.g., through infiltration or aeration), sulfur-oxidizing taxa could promote partial sulfide reoxidation, potentially leading to metal remobilization. Therefore, long-term stability is likely governed by the dynamic balance between these functional guilds, emphasizing the importance of sustained redox control at field scale.

Collectively, these results demonstrate that CPS application not only modifies geochemical conditions but also reshapes microbial community structure, fostering redox-active consortia that may enhance metal sulfide formation and redox buffering capacity. These findings highlight the importance of integrating microbial monitoring into sulfur-based remediation design, particularly in systems where sustained redox control and microbial resilience are critical for long-term stabilization efficacy.

4. Field implications

Field-scale application of CPS requires design strategies that account for limited reagent mobility and soil heterogeneity observed in column tests. Multi-point or pressurized injections may enhance uniform distribution while minimizing localized precipitation. Although moderate reductions in hydraulic conductivity (K) were observed under the coarse-textured conditions in this study, field heterogeneity and higher contaminant loads may amplify permeability losses; thus, preliminary permeability assessments and controlled injection protocols are essential. Therefore, preliminary permeability assessment, controlled injection protocols, and site-specific pilot testing with hydraulic monitoring are essential to ensure sustainable flow and long-term effectiveness during CPS implementation. Real-time monitoring of pH, ORP, Fe^{2+}, and SO_4^{2-} can support adaptive dosing to maintain sulfide availability and minimize clogging. Microbial enrichment of sulfur- and iron-metabolizing taxa observed in reactive zones suggests potential for biologically mediated stabilization, warranting inclusion of microbial assessments in site evaluations. Collectively, these insights provide a technical basis for field implementation and ongoing validation under acidic–oxidizing groundwater conditions.

5. Summary and conclusions

With respect to the six stated objectives of this study, the following conclusions can be drawn. First, CPS transport within site-specific soil is governed by gravitational settling, hydraulic gradients, and texture of the porous medium. CPS migration was confined primarily near the injection zone due to a combination of factors including localized pore clogging from early-stage precipitation and increased textural complexity of the site-specific soil. This localized injection resulted in the formation of metal sulfides ($MeS_{(s)}$) and secondary minerals such as gypsum in localized zones. In contrast to previous results obtained using a model sand, CPS exhibited limited vertical migration and preferential

lateral accumulation in lower-permeability zones. These findings highlight the critical role of soil texture in controlling CPS dispersion and the development of reactive zones in subsurface environments.

Second, CPS injection induced only moderate reductions in overall hydraulic conductivity (K), with the total K declining by a factor of 1.37. Precipitation-induced clogging, while evident in specific zones, did not significantly impede groundwater flow across the entire column. These results suggest that CPS can be applied without inducing excessive flow obstruction where the site conditions are similar to those evaluated in this study. However, increased heterogeneity and finer-grained soils in field settings may elevate clogging risk, underscoring the need for pilot-scale validation and hydraulic monitoring prior to full-scale implementation.

Third, effluent data and mass balance analyses revealed that the reactive retention time of CPS varied by metal. Cadmium removal was sustained throughout the experiment at $>$ 99 %, whereas Zn and Mg reached maximum removals of 72 % and 42 %, respectively, before rebounding. The cumulative mass removal confirmed metal-specific precipitation thresholds and depletion of reactive sulfide species as primary limiting factors. These results highlight the importance of optimizing the CPS dosage to ensure adequate contact time and reagent availability for target contaminants, particularly in complex multi-metal plumes.

Fourth, the CPS performance was significantly reduced in site-specific soil relative to previous results based on model porous media, primarily due to geochemical complexity. For example, the maximum contaminant removals of $>$ 99 %, 72 %, and 42 % for Cd, Zn, and Mg, respectively, in this study were lower than the values reported by Joo et al. [17] for model porous media, where Zn removal exceeded 99 % in clean sand. The reduced performance is attributed to competitive interactions with co-occurring metals and anions, as well as the influence of geochemical complexity and spatially variable CPS migration. This result emphasizes the need to consider real-world soil and groundwater conditions including adsorbed metal phases, mineralogical composition, and ion competition when designing CPS-based remediation strategies. Laboratory findings using clean media may overestimate field performance, and should be complemented by site-representative testing.

Fifth, the K_{sp} of metal sulfides was critical in determining CPS removal efficiency and longevity. Metals forming low-solubility, i.e., low K_{sp}, sulfides such as $CdS_{(s)}$ and $ZnS_{(s)}$ were preferentially removed, while Mg, which forms unstable or soluble sulfide and or (hydr)oxide species, exhibited limited sequestration. The results emphasize that K_{sp} values can guide reagent selection and dosing for target metals. However, CPS removal efficiency and longevity will depend on not only K_{sp} but also site-specific parameters such as pH, redox potential (ORP), and the presence of competing ions.

Sixth, microbial analysis revealed substantial shifts in community composition in CPS-reactive zones, with enrichment of sulfur- and iron-metabolizing taxa such as *Alicyclobacillus* and *Desulfitobacterium*. These microorganisms likely contributed to sulfur cycling and the stabilization of metal sulfides through redox-mediated transformations. The findings suggest that CPS injection not only alters geochemical conditions but also establishes biogeochemical feedback loops that may enhance or modify the longevity and stability of immobilized contaminants. Understanding these microbial dynamics may be important for evaluating long-term performance and sustainability of CPS-based remediation.

Although this study offers key insights into CPS transport, reactivity, and multi-metal removal under acidic-oxidizing conditions, several limitations remain. The findings are based on a short-term column test and should be validated through field-scale studies to assess long-term stability under variable redox conditions. Hydraulic heterogeneity, mineralogical variability, and microbial mediation were not fully captured, and mineral identification relied mainly on indirect geochemical evidence. Future work integrating field validation, reactive transport modeling, and microbial characterization will further elucidate CPS performance and long-term sustainability in complex natural systems.

CRediT authorship contribution statement

Charles D. Shackelford: Writing – review & editing, Writing – original draft, Validation, Software, Methodology, Investigation. **Kyoungphile Nam:** Validation, Supervision, Project administration, Funding acquisition. **Hee Sun Moon:** Resources, Project administration, Funding acquisition, Data curation. **Dong Jun Kim:** Methodology, Investigation, Data curation. **So-Jeong Kim:** Investigation, Data curation. **Jin Chul Joo:** Writing – review & editing, Writing – original draft, Visualization, Validation, Methodology, Investigation, Formal analysis, Data curation, Conceptualization. **Hyeon Woo Go:** Visualization, Methodology, Investigation, Formal analysis, Data curation.

Declaration of Competing Interest

The authors declare that they have no known competing financial interests or personal relationships that could have appeared to influence the work reported in this paper.

Acknowledgements

The authors thank the Institute of Engineering Research at Seoul National University for technical assistance and acknowledge the support of the Research Project “Microbial monitoring during in-situ immobilization of heavy metal-contaminated groundwater by CPS injection” (IP 2024-010) by the Korea Institute of Geoscience and Mineral Resources, which funded by Seoul National University.

Appendix A. Supporting information

Supplementary data associated with this article can be found in the online version at doi:10.1016/j.jece.2025.120217.

Data Availability

Data will be made available on request.

References

[1] M.C. Graham, J.G. Farmer, P. Anderson, E. Paterson, S. Hillier, D.G. Lumsdon, R. J. Bewley, Calcium polysulfide remediation of hexavalent chromium contamination from chromite ore processing residue, Sci. Total Environ. 364 (1-3) (2006) 32–44, https://doi.org/10.1016/j.scitotenv.2005.11.007.

[2] S. Petersen, K. Hedquist, Treatability test report for calcium polysulfide in the 100-K area, US Department of Energy, 2006. US DOE/RL-2006-17.

[3] California Department of Toxic Substances Control (DTSC), 2006. *Coast Wood Preserving: Third Five-Year Review*. with U.S. EPA support. (PDF) ⟨https://semspub.epa.gov/work/HQ/179404.pdf⟩.

[4] Francis J.T., 2008. *In situ* chemical reduction of hexavalent chromium at a former plating facility. In: *Proc. 6th Int. Conf. on Remediation of Chlorinated and Recalcitrant Compounds* (Monterey, CA), Paper H-039. (PDF) ⟨https://projects.battelle.org/chlorinated-conference/2008Chlor_Proceedings/Papers/H-039_Ppr.pdf⟩.

[5] M. Chrysochoou, D.R. Ferreira, C.P. Johnston, Calcium polysulfide treatment of Cr (VI)-contaminated soil, J. Hazard. Mater. 179 (1-3) (2010) 650–657, https://doi.org/10.1016/j.jhazmat.2010.03.052.

[6] M. Chrysochoou, C.P. Johnston, G.A. Dahal, A comparative evaluation of hexavalent chromium treatment in contaminated soil by calcium polysulfide and green-tea nanoscale zero-valent iron, J. Hazard. Mater. 201-202 (2012) 33–42, https://doi.org/10.1016/j.jhazmat.2011.11.003.

[7] S.M. Dahlawi, S. Siddiqui, Calcium polysulphide, its applications and emerging risk of environmental pollution—a review article, Environ. Sci. Pollut. Res. 24 (2017) 92–102, https://doi.org/10.1007/s11356-016-7842-3.

[8] T. Mpouras, N. Papassiopi, K. Lagkouvardos, C. Mystrioti, D. Dermatas, Evaluation of calcium polysulfide as a reducing agent for the restoration of a Cr (VI)-contaminated aquifer, Bull. Environ. Contam. Toxicol. 106 (2021) 435–440, https://doi.org/10.1007/s00128-020-02890-1.

[9] Cross Manufacturing Inc, Voluntary Cleanup Report: Lewis, Kansas. Kansas Dept. of Health & Environment, 215, Bureau of Environmental Remediation, 2015. ⟨https://clu-in.org/download/contaminantfocus/chromium/Cr-Reduction-Cross-KS-2015.pdf⟩ (PDF).

[10] Tetra Tech, Inc, 2018. *In-Situ Chromium Treatability Study Results Report*, Nevada Environmental Response Trust (NERT) Site, Henderson, NV. (PDF) ⟨https://clu-in.org/download/contaminantfocus/chromium/Cr-NERT-Treatability.pdf⟩.
[11] K. Soya, N. Mihara, D. Kuchar, M. Kubota, H. Matsuda, T. Fukuta, Selective sulfidation of copper, zinc and nickel in plating wastewater using calcium sulfide, Int. J. Environ. Sci. Eng. 2 (2) (2010) 93–97 (Selective_Sulfidation-libre.pdf).
[12] C. Tu, F. Guan, Y. Sun, P. Guo, Y. Liu, L. Li, K.G. Scheckel, Y. Luo, Stabilizing effects on a Cd polluted coastal wetland soil using calcium polysulphide, Geoderma 332 (2018) 190–197, https://doi.org/10.1016/j.geoderma.2018.07.013.
[13] C.Y. Huang, P.C. Cheng, J.H. Chang, Y.C. Wan, X.M. Hong, S.F. Cheng, Feasibility of remediation lead, nickel, zinc, copper, and cadmium-contaminated groundwater by calcium sulfide (Article), Water 13 (16) (2021) 2266, https://doi.org/10.3390/w13162266.
[14] H.U. Rahim, M. Qaswar, M. Wang, X. Jing, X. Cai, Environmental applications of reduced sulfur species and composites in transformation and detoxification of contaminants, J. Environ. Chem. Eng. 9 (6) (2021) 106696, https://doi.org/10.1016/j.jece.2021.106696.
[15] H.W. Go, J.C. Joo, K. Nam, H.S. Moon, S. Yoon, D.H. Lee, S.Y. Jang, Feasibility evaluation for remediation of groundwater contaminated with heavy metal using calcium polysulfide in homogeneous media, J. Soil Groundw. Environ. 28 (1) (2023) 1–14, https://doi.org/10.7857/JSGE.2023.28.1.001.
[16] S. Yoon, S. Jeong, C. Moon, K. Nam, Removal of cadmium and zinc by calcium polysulfide in acidic groundwater: Injection ratio and precipitation mechanism, Chemosphere 364 (2024) 143219, https://doi.org/10.1016/j.chemosphere.2024.143219.
[17] J.C. Joo, H.W. Go, C.D. Shackelford, K. Nam, H.S. Moon, J. Choi, J. Kim, Remediating zinc-contaminated groundwater with calcium polysulfide using model porous media and simulated groundwater, J. Hazard. Mater. 491 (2025) 137840, https://doi.org/10.1016/j.jhazmat.2025.137840.
[18] Orion Environmental Inc, 2018. *Orion performed in-situ chemical reduction for treating heavy metals in groundwater*. Available at: ⟨https://www.orionenv.com/orion-performed-in-situ-chemical-reduction-for-treating-heavy-metals-in-groundwater/⟩ (accessed 2025-10-10).
[19] X. Zhang, L. Zeng, Y. Wang, J. Tian, J. Wang, W. Sun, H. Han, Y. Yang, Selective separation of metals from wastewater using sulfide precipitation: A critical review in agents, operational factors and particle aggregation, J. Environ. Manag. 344 (2023) 118462, https://doi.org/10.1016/j.jenvman.2023.118462.
[20] ASTM, Standard practice for classification of soils for engineering purposes (Unified Soil Classification System). ASTM D2487-17e1, ASTM, West Conshohocken, PA, 2020, https://doi.org/10.1520/D2487-17E01.
[21] NIER (National Institute of Environmental Research in Korea), Standard Method for Soil Contamination Testing, National Institute of Environmental Research, Korea, 2012.
[22] KMOE (Ministry of Environment, Korea), Soil Environment Conservation Act in Korea, Ministry of Environment, Sejong, Republic of Korea, 2016. ⟨https://elaw.klri.re.kr/eng_service/lawView.do?hseq=46236&lang=ENG⟩ (accessed 2025-10-10).
[23] Y. Wang, T. Chen, K. Yeh, M. Shue, Stabilization of an elevated heavy metal contaminated site, J. Hazard. Mater. 88 (1) (2001) 63–74, https://doi.org/10.1016/S0304-3894(01)00289-8.
[24] S. Xue, W. Ke, J. Zeng, C.B. Tabelin, Y. Xie, L. Tang, C. Xiang, J. Jiang, Pollution prediction for heavy metals in soil-groundwater systems at smelting sites, Chem. Eng. J. 473 (2023) 145499, https://doi.org/10.1016/j.cej.2023.145499.
[25] A.E. Lewis, Review of metal sulphide precipitation, Hydrometallurgy 104 (2) (2010) 222–234, https://doi.org/10.1016/j.hydromet.2010.06.010.
[26] USEPA (United States Environmental Protection Agency), 2005, Pesticides and Other Toxic Substances. Reregistration eligibility decision for inorganic polysulfides. List D—case no. 4054. (Sep 30, 2005). ⟨https://archive.epa.gov/pesticides/reregistration/web/pdf/inorganic_polysulfides_red.pdf⟩.
[27] Y.-X. Xie, W.-C. Cheng, L. Wang, Z.-F. Xue, M.M. Rahman, W. Hu, Immobilizing copper in loess soil using microbial-induced carbonate precipitation: Insights from test tube experiments and one-dimensional soil columns, J. Hazard. Mater. 444 (2023) 130417, https://doi.org/10.1016/j.jhazmat.2022.130417.
[28] W.M. Seo, M.N. Riffel, A.G. Oliver, E.Y. Tsui, Metal-cation-induced shifts in thiolate redox and reduced sulfur speciation, Chem. Sci. 15 (19) (2024) 7332–7341, https://doi.org/10.1039/d4sc01025f.
[29] D. Rickard, G.W. Luther III, Metal sulfide complexes and clusters, Rev. Miner. Geochem 61 (1) (2006) 421–504, https://doi.org/10.2138/rmg.2006.61.8.
[30] A. Pohl, Removal of heavy metal ions from water and wastewaters by sulfur-containing precipitation agents, Water Air Soil Pollut. 231 (2020) 503, https://doi.org/10.1007/s11270-020-04863-w.
[31] H. Estay, L. Barros, E. Troncoso, Metal sulfide precipitation: recent breakthroughs and future outlooks, Minerals 11 (12) (2021) 1385, https://doi.org/10.3390/min11121385.
[32] S.W. Poulton, M.D. Krom, R. Raiswell, A revised scheme for the reactivity of iron (oxyhydr)oxide minerals towards dissolved sulfide, Geochim. Cosmochim. Acta 68 (18) (2004) 3703–3715, https://doi.org/10.1016/j.gca.2004.03.012.
[33] X. Guo, X.-Y. You, L.-J. Liu, J.-Y. Zhang, S.-J. Liu, C.-Y. Jiang, Alicyclobacillus aeris sp. nov., a novel ferrous- and sulfur-oxidizing bacterium isolated from a copper mine, Int. J. Syst. Evol. Microbiol 59 (10) (2009) 2415–2420, https://doi.org/10.1099/ijs.0.008870-0.
[34] F. Arsène-Ploetze, S. Koechler, M. Marchal, et al., Structure, function, and evolution of the Thiomonas spp. Genome, PLoS Genet. 6 (2) (2010) e1000859, https://doi.org/10.1371/journal.pgen.1000859.